NANO LETTERS

LETTER

pubs.acs.org/NanoLett

Controlling the Morphology of Rhodium Nanocrystals by Manipulating the Growth Kinetics with a Syringe Pump

Hui Zhang,[†,‡] Weiyang Li,[†] Mingshang Jin,[†] Jie Zeng,[†] Taekyung Yu,[†] Deren Yang,[‡] and Younan Xia*[,†]

[†]Department of Biomedical Engineering, Washington University, St. Louis, Missouri 63130, United States

[‡]State Key Laboratory of Silicon Materials and Department of Materials Science and Engineering, Zhejiang University, Hangzhou, Zhejiang 310027, People's Republic of China

Supporting Information

ABSTRACT: Noble-metal nanocrystals with well-defined and controllable morphologies are of great importance to applications in catalysis, plasmonics, and surface-enhanced spectroscopy. Many synthetic approaches have been demonstrated for controlling the growth habit and thus morphology of metal nanocrystals, but most of them are based on a thermodynamic approach, including the use of a capping agent. While thermodynamic control has shown its power in generating nanocrystals with a myriad of different morphologies, it is ultimately limited by the obligation to minimize the surface energy of a system. As a result, it is impractical to use thermodynamic control to generate nanocrystals having high-energy facets and/or a negative curvature. Using rhodium as an example, here we demonstrate a general method based on kinetic control with a syringe pump that can be potentially extended to other noble metals and even other solid materials. For the first time, we were able to produce concave nanocubes with a large fraction of {110} facets and octapods with a cubic symmetry in high yields by simply controlling the injection rate at which the precursor was added into the reaction solution. The concave nanocubes with {110} facets and a unique cavity structure on the surface are important for a variety of applications.

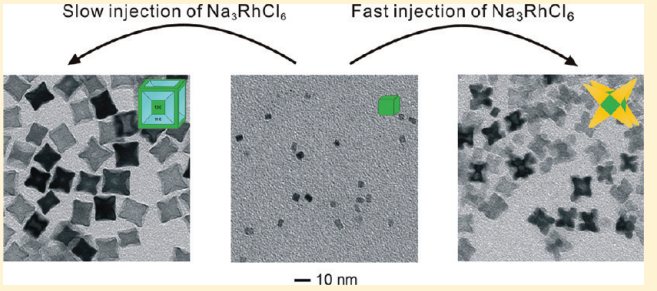

KEYWORDS: Kinetic control, concave nanocubes, rhodium, injection rate, bimetallic

Maneuvering the morphology of noble-metal nanocrystals offers a powerful means to tailor their properties for enhanced performance in a rich variety of applications.[1−5] In general, both thermodynamic and kinetic approaches can be employed to control the morphology of a nanocrystal.[6,7] The thermodynamic control, including the use of a capping agent, is based on the requirement to minimize the total surface energy of a system. It is most successful in generating nanocrystals that are enclosed by a convex surface and low-energy facets, with typical examples including cube, octahedron, tetrahedron, cuboctahedron, decahedron, and icosahedron.[8] In contrast, the kinetic control is based on manipulation of growth rate at which atoms are generated and added to the surface of a growing seed. The product of kinetically controlled growth is not confined by thermodynamics; notable examples include nanocrystals enclosed by high-energy facets and/or with a concave structure on the surface.[9−12]

Although kinetic control can potentially generate novel nanocrystals with unusual shapes, high-energy facets, and/or a negative surface curvature, it has not been easy to implement the concept experimentally. In general, the reaction kinetics involved in a nanocrystal synthesis can be manipulated by controlling all the reaction conditions, including reagent concentration, temperature, type of reductant, addition of ionic species, or a combination of them. For example, Yang and co-workers have demonstrated the synthesis of Au nanocrystals with truncated tetrahedral or icosahedral shapes by varying the concentration of the precursor.[13] We have demonstrated the synthesis of Pd nanoplates instead of cuboctahedrons (a shape favored by thermodynamics) by varying the temperature and using different reductants.[14,15] In addition, we and other groups have developed an effective strategy for kinetically controlling the morphology of noble-metal nanocrystals by introducing an oxidative etchant such as Cl^-/O_2, Fe^{II}/Fe^{III}, and Cu^{I}/Cu^{II} to retard the growth kinetics.[16−18] Besides the effect on reaction rate, however, changing the aforementioned reaction parameters may also bring in unexpected complications and thereby difficulties in controlling the morphology of final products. For example, varying the concentration and temperature may cause changes to the thermodynamic parameters of a reaction system, and thus alter the outcomes of nucleation and growth.[19] As a result, it is a grand challenge in implementing kinetic control in different systems to

Received: December 14, 2010
Revised: December 25, 2010
Published: December 30, 2010

produce nanocrystals with unusual morphologies, including those with high-energy facets and/or a negative curvature on the surface.

With rhodium (Rh) as an example, here we demonstrate a simple and convenient method for kinetic control that can be easily implemented and potentially applied to other noble metals. We chose Rh as our initial focus because nanocrystals made of this metal have received great interests as catalysts in a wide variety of reactions.[20,21] The synthesis is based on a modified polyol process that involves injection of Na_3RhCl_6 into ethylene glycol (EG) held at 140 °C with ascorbic acid (AA) and Br^- ions serving as reducing and capping agents, respectively (see Supporting Information for experimental details). We were able to achieve a kinetic control by simply adjusting the injection rate at which the Na_3RhCl_6 precursor was introduced because this precursor seemed to be immediately reduced into Rh atoms by AA upon addition into the reaction solution. To single out the effect of reaction kinetics on the morphology of product, we intentionally separated growth from nucleation by injecting a small amount of the precursor at one rate to generate the seeds, followed by the injection of a much larger amount of the precursor for growth purpose. No matter what injection rate we used for the nucleation step, a slow injection rate in the second step promoted growth along the ⟨111⟩ and ⟨110⟩ directions to form nanocubes with a concave structure. In comparison, a fast injection rate in the second step resulted in the formation of octapods with a cubic symmetry via accelerated growth along the ⟨111⟩ directions. Significantly, this new approach could also be extended to generate Pt−Rh bimetallic, concave nanocubes.

In a typical synthesis, Na_3RhCl_6 and PVP were dissolved separately in EG and then injected (using a syringe pump) simultaneously and at the same rate into another EG solution containing KBr and AA (held at 140 °C). The color of the solution turned from rose pink to dark brown immediately upon addition of the precursor, suggesting very fast reduction of Na_3RhCl_6 by AA. Figure 1a−d shows a series of TEM images taken from samples that were obtained at different stages of a synthesis with an injection rate of 4 mL/h. In the nucleation stage of the reaction (Figure 1a, 0.4 mL at t = 0.1 h), we observed a large number of Rh nanocubes of 3−4 nm in size. The magnified TEM image (inset of Figure 1a) shows that the nanocube was slightly truncated at corners and bounded by a mix of {100} and {111} facets. The formation of Rh nanocubes can probably be attributed to the preferential chemisorption of Br^- ions on {100} rather than other facets.[22,23] These nanocubes then served as seeds in the growth process. As the amount of the precursor was increased to 1 mL (Figure 1b, t = 0.25 h), the nanocubes increased to 7 nm in edge length. A careful analysis indicates that the newly formed Rh atoms were preferentially added to the corners and edges of most cubic seeds to generate nanocubes with a concave structure (inset of Figure 1b). In addition, there were still a small amount of normal cubes coexisting with the concave structures at this stage (indicated by arrows, Figure S1a of Supporting Information). This observation suggests a morphological transition from nanocubes with truncated corners to perfect nanocubes and then concave nanocubes as the amount of the precursor was increased at a slow injection rate. After 2 mL of the precursor was added (Figure 1c, t = 0.5 h), the product became dominated by concave nanocubes with {110} and {100} facets exposed on the surface. Because of an increase in size, the concave structure became more obvious under TEM

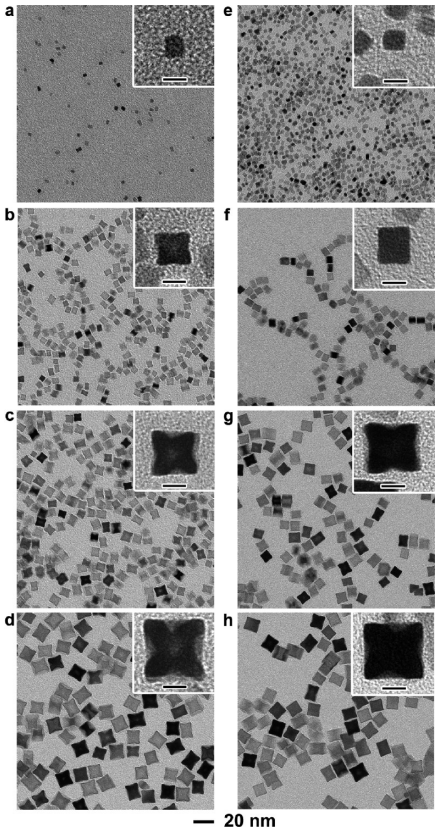

Figure 1. TEM images of Rh nanocrystals that were obtained under two different injection modes. (a−d) Slow plus slow injection, and (e−h) fast plus slow injection. The "slow" and "fast" correspond to injection rates of 4 mL/h and 60 mL/h, respectively. The images in (a−d) show TEM images of Rh nanocrystals that were obtained after different volumes of the precursor had been injected: (a) 0.4, (b) 1, (c) 2, and (d) 6 mL. The images in (e−h) show TEM images of Rh nanocrystals that were obtained after different volumes of the precursor had been added: (e) 1, (f) 6, (g) 14, and (h) 30 mL. The insets show TEM images of individual nanocrystals at a higher magnification. The scale bars in the insets are 5 nm.

(Supporting Information Figure S1b). When the amount of precursor was increased to 6 mL (Figure 1d, t = 1.5 h, and subsequently aged for 0.5 h), high-quality concave nanocubes of 15 nm in size were obtained. Further extension of the aging time to 20 h (Supporting Information Figure S1c) did not lead to any obvious change in size and morphology for the concave nanocubes because the supply of precursor had already been terminated. Supporting Information Figure S1d shows the average edge lengths of Rh nanocubes obtained at different stages of the synthesis. The data were obtained from 100 nanocrystals randomly selected from TEM images (see Supporting Information Figure S2 for size distributions). The plot indicates that the edge length of the Rh nanocubes linearly increased from 3 to 15 nm when the volume of the precursor was increased from 0.4 mL (t = 0.1 h) to 6 mL (t = 1.5 h, and subsequently aged for 0.5 h). However, the size remained essentially the same during the aging process after t = 2 h, indicating that the precursor was immediately reduced and added to the surface of growing seeds, and no other growth mechanisms such as oriented attachment of small nanoparticles and Ostwald ripening were involved. This observation also suggests that the concave structure could be preserved during an aging process.

dx.doi.org/10.1021/nl104347j |*Nano Lett.* 2011, 11, 898–903

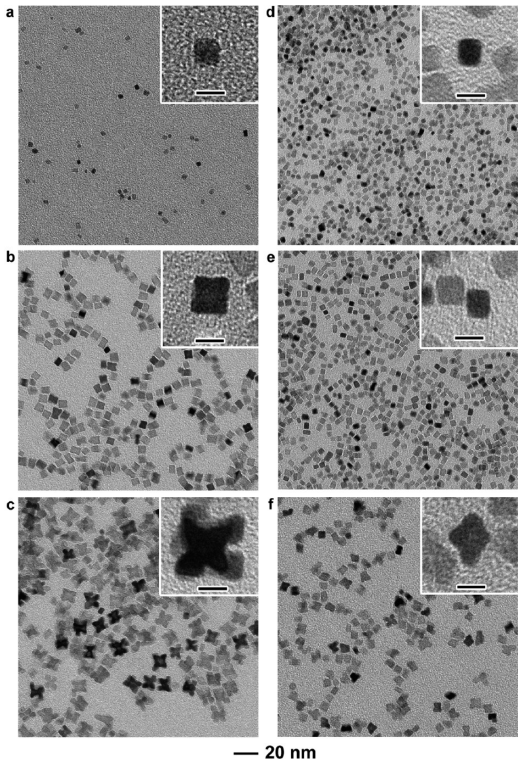

Figure 2. TEM images of Rh nanocrystals that were obtained under two additional different injection modes. (a−c) Slow plus fast injection and (d−f) fast plus fast injection. The "slow" and "fast" correspond to injection rates of 4 mL/h and 60 mL/h, respectively. The images in (a−c) show TEM images of Rh nanocrystals that were obtained after different volumes of the precursor had been injected: (a) 0.4, (b) 1, and (c) 6 mL. The images in (d−f) show TEM images of Rh nanocrystals that were obtained after different volumes of the precursor had been added: (d) 1, (e) 2, and (f) 6 mL. The insets show TEM images of individual nanocrystals at a higher magnification. The scale bars in the insets are 5 nm.

When we increased the injection rate to 60 mL/h between t = 0 and 1 min and then reduced the injection rate to 4 mL/h, the resultant Rh nanocrystals still evolved from truncated nanocubes to normal nanocubes with sharp corners and then concave nanocubes. Figure 1e−h shows a series of TEM images of Rh nanocrystals that were sampled after different volumes of the precursor had been added. Although high-quality concave nanocubes were still obtained in this case, the amount of the precursor required for generating Rh nanocrystals of similar sizes was increased by roughly five times in comparison to those involving slow injection only. Obviously, a faster injection rate (60 vs 4 mL/h) at the beginning resulted in a larger number of seeds in the solution. As a result, a larger amount of the precursor would be needed in order to generate concave nanocubes with a specific size. As shown in Figure S3, experiments data involving different amounts of the precursor in the nucleation step provides further evidence to support this argument. By reducing the amount of the precursor added in the initial step from 0.9 to 0.1 mL while keeping the total volume (6 mL) of the precursor unchanged in the entire synthesis, the final product changed from normal nanocubes with sharp corners to concave nanocubes. Taken together, we conclude that the final morphology exhibited by the Rh nanocrystals is only sensitive to the injection rate used in the growth step, rather than the nucleation step. Concave nanocubes could always be obtained at a relatively slow injection rate (4 mL/h) for the growth step, although they might appear at different stages of a synthesis (i.e., after different volumes of the precursor had been added) depending on the number of seeds formed in the nucleation step.

When we increased the injection rate for the growth step, we observed a set of completely different morphologies. Figure 2a−c shows TEM images of Rh nanocrystals prepared with an initial injection rate of 4 mL/h until t = 0.1 h and then increased to 60 mL/h. In the initial step (Figure 2a, t = 0.1 h), truncated nanocubes were observed as the primary product, which evolved into nanocubes with tiny tips at the corners when 1 mL of the precursor was added (Figure 2b, t = 0.25 h). This morphology was similar to what was observed in Figure 1b. In the next stage, Rh octapods with a cubic symmetry (Figure 2c) were formed due to accelerated growth along the ⟨111⟩ directions from the corners of a cubic seed. The low-magnification TEM image clearly shows that most of the nanocrystals were composed of eight arms. The arms were 2−5 nm in width and 6−8 nm in length, whereas the overall edge length of the nanocrystals was on the order of 15 nm. When we used a fast plus fast injection mode, a large number of truncated cubic seeds were formed in the initial stage (Figure 2d), which then evolved into nanocubes with sharp corners (Figure 2e) after 2 mL of the precursor had been injected at a fast rate. Subsequently, these nanocrystals also evolved into octapods with a cubic symmetry (Figure 2f) due to preferential growth along the ⟨111⟩ directions. Compared with the slow plus fast mode, however, the octapods obtained under the fast plus fast mode were still in a rudimentary state due to the substantially increased number of seeds in the solution. It can be concluded that the Rh nanocrystals in the two aforementioned injection modes followed the same growth pattern.

Since the concave, cubic structure represents a new morphology, we fully characterized its structure by TEM and high-resolution TEM. In general, the concave nanocrystals exhibited a darker contrast in the center as compared with the edges when imaged by TEM. Figure 3a,b gives additional TEM images of the sample shown in Figure 1d. The images clearly show that about 90% of the nanocubes had a concave structure with a square or rectangular projection due to different orientations relative to the electron beam. The concave structure was also supported by SEM images (see the insets of Figure 1a and Supporting Information Figure S4a). In general, when a concave nanocube is projected along the [100], [110], and [111] zone axes, respectively, we expect to observe square, rectangular, and hexagonal profiles (Supporting Information Figure S4b−d). Careful examination of the nanocrystal in Supporting Information Figure S4b indicates that the image projected along the [100] axis consisted of a square of 3−4 nm in edge length in the center (corresponding to the initial seed), four trapezium regions (the concave portion), and a diagonal cross of 3−4 nm in thickness that was formed due to overgrowth along the ⟨111⟩ and ⟨110⟩ directions. From these TEM and SEM studies, we can conclude that the concave nanocubes were different from the previously reported Pt octapods characterized by a cubic symmetry.[24] Figure 3c−e shows high-resolution TEM images of individual concave Rh nanocubes along the [100], [110], and [111] zone axes, respectively. These images clearly show well-resolved, continuous fringes with the same orientation, indicating that the concave nanocubes were single crystals. The fringes with lattice spacing of 2.21, 1.91, and 1.35 Å can be indexed to the {111}, {200}, and {220} planes of face-centered cubic Rh,

dx.doi.org/10.1021/nl104347j |*Nano Lett.* 2011, 11, 898–903

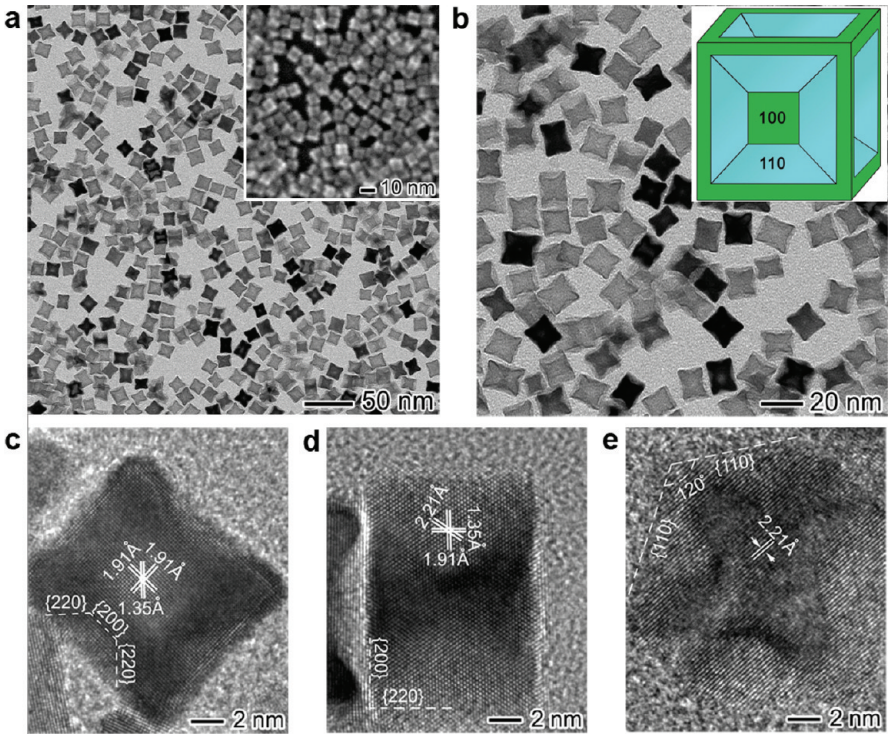

Figure 3. Morphological and structural characterizations of a typical sample of Rh concave nanocubes prepared at 140 °C with an injection mode of slow plus slow. The "slow" here corresponds to an injection rate of 4 mL/h. (a,b) TEM images of the as-prepared sample and (c−e) HRTEM images of individual concave nanocubes recorded along the [100], [110], and [111] zone axes. The insets in (a) and (b) show a typical SEM image of the concave nanocubes and the 3D model, respectively.

respectively. As a result, the side surface of the concave region is bounded by a mix of both {100} and {110} facets. On the basis of the TEM, SEM, and HRTEM analyses, we can propose a three-dimensional model as shown in the inset of Figure 3b. The model can be visualized as a concave cube with a truncated square pyramid excavated at the center of each face of the cube. Each concave nanocube is consisted of six square {100} faces, six square {100} faces with a larger area and a square hole in the center, and 16 isosceles trapezium-like {110} side faces.

In addition to the injection rate, we also systematically investigated the effects of other reaction parameters on the morphology of resultant Rh nanocrystals. The slow plus slow injection mode was used as a representative system. In the absence of AA (Figure 4a), both concave nanocubes and irregular nanoparticles (marked by arrows) were obtained. Although the exact mechanism is yet to be elucidated, the difference in reduction power between AA and EG might be responsible for the different growth habits. Under Ar protection (Figure 4b), concave nanocubes and some twinned multipods (marked by arrows) were obtained. The formation of twinned multipods is understandable because the oxidative etching power of the Cl^-/O_2 pair was reduced due to the exclusion of air by an inert gas.[14] When the Na_3RhCl_6 precursor was replaced by $Rh(NO_3)_3$, concave nanocubes of 12 nm in size were obtained (Figure 4c). A small number of twinned, starfishlike nanocrystals (marked by arrows) also coexisted with the concave nanocubes in the final product. The weaker coordination power of NO_3^- than Cl^- for oxidative etching might be responsible for the formation of smaller concave nanocubes and starfishlike nanocrystals because a much larger number of seeds (both single-crystal and twinned) could be formed in the nucleation stage. In the absence of KBr

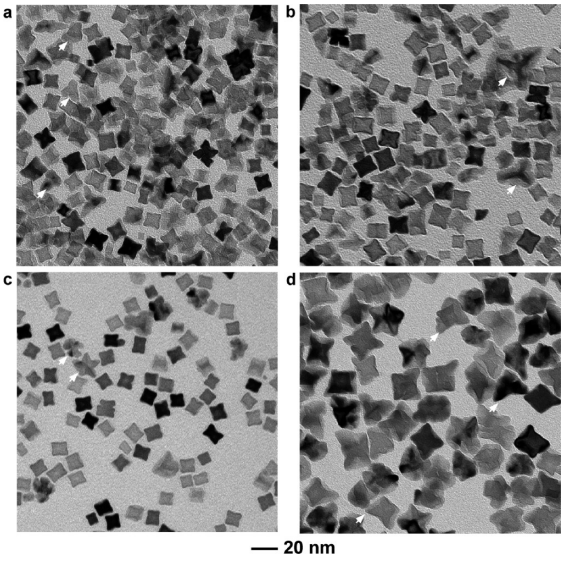

Figure 4. TEM images of Rh nanocrystals prepared under slow plus slow injection mode at 140 °C for 2 h: (a) in the absence of ascorbic acid, (b) under Ar protection, (c) with $Rh(NO_3)_3$ instead of Na_3RhCl_6 as a precursor, and (d) in the absence of KBr. All other parameters were kept the same as the standard synthesis. The "slow" here corresponds to an injection rate of 4 mL/h. The arrows indicate Rh nanoparticles with a irregular shape or a multiple twinned structure commonly formed in the absence of oxidative etching.

(Figure 4d), irregular nanoparticles were obtained because growth along the ⟨100⟩ directions was not retarded by the capping agent of Br^-. There were also some bumps protruding

dx.doi.org/10.1021/nl104347j |*Nano Lett.* 2011, 11, 898–903

from the irregular nanoparticles (marked by arrows). These bumps were a result of fast growth along the ⟨111⟩ directions, which was also observed in our most recent work on the synthesis of Rh multipods.[25] We also conducted a systematic investigation on this parameter (Supporting Information Figure S5). As the amount of KBr was increased from 0.0024 to 3.6 mmol, the concave nanocubes were produced at increasing yields. These results indicated that Br^- ions played an important role in shaping a cubic profile for the Rh nanocrystals by selectively passivating the {100} facets. The chemisorption of Br^- ions on the {100} facets also greatly blocks the addition of Rh atoms to the {100} facets of a growing seed, facilitating overgrowth at corners and edges.

Supporting Information Figure S6 shows a summary of morphological changes involved in the evolution of Rh nanocrystals as more precursors was introduced under four different modes. In general, the formation of nanocrystals can be separated into two basic steps, nucleation and growth. As shown by the results in Figures 1 and 2, the injection rate used for the growth step plays the most important role in determining the final morphology. For the nucleation step, a faster injection rate only results in a larger number of seeds, and thus a larger volume of the precursor needed to generate nanocrystals with a specific size. As a result, the four injection modes can be grouped into two categories according to the injection rate used in the growth step. When Na_3RhCl_6 is injected into an EG solution containing AA and KBr, this precursor will be immediately reduced into Rh atoms by AA upon addition. The Rh atoms initially nucleated and formed small cubic seeds of Rh due to the selective adsorption of Br^- on the {100} facets. For a nanocrystal seed with a cubic shape, the reactivity is supposed to decrease in the order of corner, edge, and side face. This difference in reactivity can be amplified due to the selective adsorption of Br^- on the {100} side faces. As such, Rh atoms generated from the injected precursor in the growth step were expected to preferentially diffuse onto the most active sites (eight corners) of a cubic seed (the arrival step in Supporting Information Figure S7). After that, the Rh atoms at corners could stay to grow along the ⟨111⟩ directions (the growth step in Supporting Information Figure S7) or migrate to other sites such as edges and side faces through surface diffusion. The ratio of atoms associated with these two types of growth modes should be mainly determined by the concentration of Rh atoms, and thus the injection rate for the precursor. Since the {100} facets were blocked by Br^- ions, the Rh atoms could only migrate from corners to edges on a cubic seed (see Supporting Information Figure S7). At a fast injection rate, the Rh atoms around corners were always retained at a high supersaturation. As a result, growth along the ⟨111⟩ directions was accelerated relative to the ⟨110⟩ directions as only a small number of Rh atoms could have enough time to to migrate to the edges. Since growth only occurred slightly at edges along the ⟨110⟩ directions, the final product evolved into octapods with a cubic symmetry. When the injection rate was slow enough, it would take a relatively long time to achieve a high level of supersaturation around the corners of a cubic seed. During this period, most of the Rh atoms at corners should have enough time to migrate to edges through surface diffusion. As a result, the cubic seed would grow at both corners and edges along the ⟨111⟩ and ⟨110⟩ directions, respectively, with a similar rate. The final product would become concave nanocubes.

We have also demonstrated the synthesis of Pt−Rh bimetallic, concave nanocubes (Figure 5) by manipulating the growth kinetics in a seed-mediated process involving two different metals.

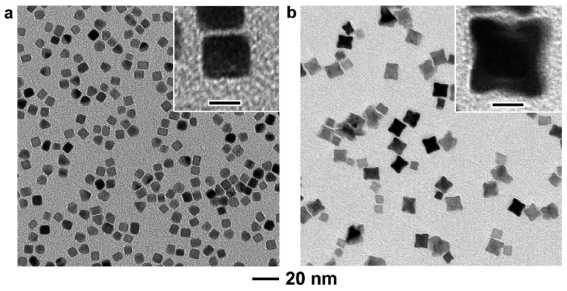

Figure 5. TEM images of cubic Pt seeds and Pt−Rh concave nanocubes. (a) TEM image of Pt nanocubes that were synthesized by reducing Na_2PtCl_6 with ethylene glycol (held at 198 °C) at an injection rate of 60 mL/h and in the presence of Br^- as a capping agent. (b) TEM image of Pt−Rh concave nanocubes that were obtained by injecting (at a rate of 4 mL/h) Na_3RhCl_6 into ethylene glycol (held at 140 °C) that contained the cubic Pt nanocrystals (as seeds), KBr (as a capping agent), and ascorbic acid (as a reductant). The insets show TEM images of individual nanocrystals at a higher magnification. The scale bars in the insets are 5 nm.

In this case, cubic Pt seeds (Figure 5a) were generated by introducing a Pt precursor into EG (held at 198 °C) at an injection rate of 60 mL/h (fast injection) and in the presence of Br^- ions as a capping agent. This procedure was similar to what was reported in a recent publication.[20] The as-prepared Pt cubes were then used as seeds to grow Pt−Rh bimetallic concave nanocubes (Figure 5b) by injecting the Na_3RhCl_6 precursor at a rate of 4 mL/h (slow injection) at 140 °C and in the presence of KBr and ascorbic acid, using a procedure similar to what was used in Figure 1b−d. The final product showed a cubic shape, together with a concave structure.

In summary, we have demonstrated a simple and versatile method for controlling the morphology of nanocrystals with unusual facets and a negative curvature by manipulating the reaction kinetics. The key to the success of this synthesis is to control the rate at which the precursor is added into a growth solution to selectively enhance overgrowth of cubic seeds from corners and edges along ⟨111⟩ and ⟨110⟩ directions, respectively, with Br^- serving as a capping agent for {100} facets. By injecting the precursor into a reaction solution with a syringe pump and at a slow (4 mL/h) or fast (60 mL/h) rate, we deterministically obtained concave nanocubes and octapods with a cubic symmetry. The concave nanocubes are bounded by a mix of both {110} and {100} facets, where the presence of a high fraction of {110} facets on the surface is attractive for applications in catalysis. We believe that the approach presented here can also be extended to other noble metals and their combinations.

■ ASSOCIATED CONTENT

Supporting Information. Experimental details and additional figures. This material is available free of charge via the Internet at http://pubs.acs.org.

■ AUTHOR INFORMATION

Corresponding Author

*E-mail: xia@biomed.wustl.edu.

■ ACKNOWLEDGMENT

This work was supported in part by a DOE subcontract from the University of Delaware (DE-FG02-03 ER15468), a research

grant from the NSF (DMR-0804088), and startup funds from Washington University in St. Louis. As a visiting scholar, H.Z. was also partially supported by the "New Star Program" of Zhejiang University, People's Republic of China. Part of the research was conducted at the Nano Research Facility (NRF), a member of the National Nanotechnology Infrastructure Network (NNIN), which is supported by the NSF under award ECS-0335765.

REFERENCES

(1) Ahmadi, T. S.; Wang, Z. L.; Green, T. C.; Henglein, A.; El-Sayed, M. A. *Science* **1996**, *272*, 1924.
(2) Burda, C.; Chen, X.; Narayanan, R.; El-Sayed, M. A. *Chem. Rev.* **2005**, *105*, 1025.
(3) Lee, I.; Delbecq, F.; Morales, R.; Albiter, M. A.; Zaera, F. *Nat. Mater.* **2009**, *8*, 132.
(4) Tian, N.; Zhou, Z. Y.; Sun, S. G.; Ding, Y.; Wang, Z. L. *Science* **2007**, *316*, 732.
(5) Camden, J. P.; Dieringer, J. A.; Zhao, J.; Van Duyne, R. P. *Acc. Chem. Res.* **2008**, *41*, 1653.
(6) Xia, Y.; Xiong, Y.; Lim, B.; Skrabalak, S. E. *Angew. Chem., Int. Ed.* **2009**, *48*, 60.
(7) Tao, A.; Habas, S.; Yang, P. D. *Small* **2008**, *4*, 310.
(8) Lim, B.; Jiang, M.; Tao, J.; Camargo, P.; Zhu, Y.; Xia, Y. *Adv. Funct. Mater.* **2009**, *19*, 189.
(9) Ming, T.; Feng, W.; Tang, Q.; Wang, F.; Sun, L.; Wang, J.; Yan, C. *J. Am. Chem. Soc.* **2009**, *131*, 16350.
(10) Ma, Y.; Kuang, Q.; Jiang, Z.; Xie, Z.; Huang, R.; Zheng, L. *Angew. Chem., Int. Ed.* **2008**, *47*, 8901.
(11) Huang, X.; Tang, S.; Zhang, H.; Zhou, Z.; Zheng, N. *J. Am. Chem. Soc.* **2009**, *131*, 13916.
(12) Zhang, J.; Langille, M. R.; Personick, M. L.; Zhang, K.; Li, S.; Mirkin, C. A. *J. Am. Chem. Soc.* **2010**, *132*, 14012.
(13) Kim, F.; Connor, S.; Song, H.; Kuykendall, T.; Yang, P. *Angew. Chem., Int. Ed.* **2004**, *43*, 3673.
(14) Xiong, Y.; Chen, J.; Wiley, B.; Xia, Y.; Aloni, S.; Yin, Y. *J. Am. Chem. Soc.* **2005**, *127*, 7332.
(15) Xiong, Y.; McLellan, J. M.; Chen, J.; Yin, Y.; Li, Z. Y.; Xia, Y. *J. Am. Chem. Soc.* **2005**, *127*, 17118.
(16) Wiley, B.; Herricks, T.; Sun, Y. G.; Xia, Y. *Nano Lett.* **2004**, *4*, 1733.
(17) Chen, J. Y.; Herricks, T.; Geissler, M.; Xia, Y. *J. Am. Chem. Soc.* **2004**, *126*, 10854.
(18) Tao, A.; Sinsermsuksakul, P.; Yang, P. *Angew. Chem., Int. Ed.* **2006**, *45*, 4597.
(19) Xie, T.; Li, S. A.; Peng, Q.; Li, Y. D. *Angew. Chem., Int. Ed.* **2009**, *48*, 196.
(20) Zhang, Y.; Grass, M. E.; Kuhn, J. N.; Tao, F.; Habas, S. E.; Huang, W.; Yang, P.; Somorjai, G. A. *J. Am. Chem. Soc.* **2008**, *130*, 5868.
(21) Park, K. H.; Jang, K.; Kim, H. J.; Son, S. U. *Angew. Chem., Int. Ed.* **2007**, *46*, 1152.
(22) Lee, H.; Habas, S. E.; Kweskin, S.; Butcher, D.; Somorjai, G. A.; Yang, P. *Angew. Chem., Int. Ed.* **2006**, *45*, 7824.
(23) Xiong, Y. J.; Xia, Y. *Adv. Mater.* **2007**, *19*, 3385.
(24) Cheong, S.; Watt, J.; Ingham, B.; Toney, M. F.; Tilley, R. D. *J. Am. Chem. Soc.* **2009**, *131*, 14590.
(25) Zettsu, N.; McLellan, J. M.; Wiley, B.; Yin, Y.; Li, Z. Y.; Xia, Y. *Angew. Chem., Int. Ed.* **2006**, *45*, 1288.